# Solar variability of the daytime atomic oxygen O($^1$S) emission in the middle and lower thermosphere

Rawatee Maharaj-Sharma
University of the West Indies, St. Augustine, Trinidad and Tobago

Gordon G. Shepherd
Centre for Research in Earth and Space Science, York University, Toronto, Canada

Received 5 August 2003; revised 19 November 2003; accepted 16 January 2004; published 13 March 2004.

[1] The Wind Imaging Interferometer (WINDII) on board the Upper Atmosphere Research Satellite (UARS) measures winds from the Doppler shifts of airglow emissions, and as a by-product the volume emission rates (photon $cm^{-3}$ $s^{-1}$) of those emissions. This includes the atomic oxygen O($^1$S) emission at 557.7 nm, which during the daytime is emitted over a large altitude range from about 85 km to over 250 km. Two distinct peaks in altitude are formed, one near 100 km (herein denoted the E region) and one near 150 km (herein the F region). The daytime E region emission was virtually unknown prior to WINDII – it resembles its nighttime counterpart, but the emission rate is much higher and it is broader in vertical extent. Both regions are produced by direct and indirect processes, but the WINDII data show that both behave as Chapman layers, corresponding to production of emission by absorption of solar radiation. The F region processes are fairly well understood, but the direct E region process has not previously been identified. The data are consistent with excitation by photodissociation of $O_2$ dominantly by Lyman-β. The solar influence is investigated through correlations of daily values of emission rate with six solar indices; the E region yields higher coefficients than the F region, with the highest value for solar Ly-α at 0.82, which is consistent with the Ly-β process. For one of the six indices, the GOES xl x-rays (0.1–0.8 nm), no correlation is evident, in part because the radiances are too low to produce the observed emission, but also because the radiances are seemingly random, not following the solar cycle variation. Variations of atmospheric origin with latitude and longitude are briefly reported upon, and an F region emission rate scale height correlation with temperature is also found. *INDEX TERMS:* 0310 Atmospheric Composition and Structure: Airglow and aurora; 7536 Solar Physics, Astrophysics, and Astronomy: Solar activity cycle (2162); 0358 Atmospheric Composition and Structure: Thermosphere—energy deposition; 2423 Ionosphere: Ionization mechanisms; *KEYWORDS:* atomic oxygen, dayglow, solar indices, E region, F region, Lyman-beta

**Citation:** Maharaj-Sharma, R., and G. G. Shepherd (2004), Solar variability of the daytime atomic oxygen O($^1$S) emission in the middle and lower thermosphere, *J. Geophys. Res.*, *109*, A03303, doi:10.1029/2003JA010183.

## 1. Introduction

[2] Observations of the atomic oxygen O($^1$S) greenline dayglow emission at 557.7 nm have until the advent of satellite observations been very limited because of the dominance of Rayleigh scattering of sunlight by the atmosphere for ground-based observations. Ground-based observations of the oxygen O($^1$D) line at 630 nm were reported by *Bens et al.* [1965], and *Noxon* [1968]; a thorough review of these and other dayglow observations was compiled by *Chakrabarti* [1998]. More recent daytime measurements are presented by *Sridharan et al.* [1999], *Pallamraju et al.* [2001] and *Taori et al.* [2003]. A satellite instrument views above the region of Rayleigh scattering; this makes routine dayglow measurements feasible. The first satellite-borne instrument to observe dayglow was the Visible Airglow Experiment (VAE) on the Atmospheric Explorer satellite [*Hays et al.*, 1973]. More recently the Wind Imaging Interferometer WINDII [*Shepherd et al.*, 1993a] on board the Upper Atmosphere Research Satellite (UARS) has proven an excellent instrument for making routine dayglow observations as it is well equipped with a meter-long baffle to prevent Rayleigh and other scattered light from the lower atmosphere from entering the instrument. WINDII measures wind, temperature and volume emission rate (number of photons emitted per unit volume per second), over the altitude range 80 to 300 km by using the visible region airglow emission from these altitudes as a target and employing Doppler Michelson Imaging [*Shepherd*, 2002] to measure small wavelength shifts. WINDII consists of a field-widened Michelson interferometer, which views the


0148-0227/04/2003JA010183$09.00

Earth's limb through two fields of view; one at 45° and the other at 135° to the orbit track, from an altitude of about 585 km [*Shepherd et al.*, 1993a].

[3] WINDII observations of daytime O($^1$S) were modeled by *Singh et al.* [1996] and by *Witasse et al.* [1999]. Good agreement was found over the altitude range 130 to 200 km which is referred to herein as the "F region emission", and even better agreement was found by *Upadhayaya and Singh* [2002] using the new temperature-dependent rate coefficient for the $N_2(^3\Sigma_u^+)$ reaction derived by *Hill et al.* [2000] – indicating that the excitation processes here are well understood. *Singh and Tyagi* [2002] evaluated the emission rate for different solar irradiance levels. In the F region the daytime emission is greatly enhanced over the nighttime values because of the flux of exciting photoelectons produced by solar EUV radiation. At night, this emission is often not observed at all, except near the equator in the regions of tropical arcs [*Thuillier et al.*, 2002], where ionization levels are high. The well-known and well-studied nighttime O($^1$S) greenline emission exists in a narrow peak near 100 km, and is produced by the recombination of atomic oxygen atoms. It was therefore surprising to find in the WINDII data that this daytime "E region" emission rate was larger by a factor of three or more in the daytime than at night. The daytime excitation process is investigated here, and a mechanism proposed.

[4] The overall goal of this work is to understand the solar influence on the characteristics of the daytime O($^1$S) green line emission at 557.7 nm, and on their variability. This was done by studying the response of the emission to the solar zenith angle, and through a comparison of the emission rate with six solar indices, each reflecting different wavelengths of the solar spectrum. The first investigations of these data were carried out by *Siddiqi* [1996] and by *Shepherd et al.* [1997a]. These characteristics include the peak emission rate, the altitude of the peak, as well as the E region profile widths and F region scale height [*Maharaj-Sharma*, 2002]. The temperature variation inferred from the scale height of the greenline dayglow is compared with that from the MSIS model [*Hedin*, 1991] and the findings are shown here. The data for the 3-year period from 16 January 1992 to 23 March 1995 is used in this work, a period of decay in solar activity from just after a solar maximum to near-minimum.

## 2. Atomic Oxygen Greenline Profiles

[5] Atomic oxygen dayglow emissions are excited by both direct and indirect processes. The details for the F region are only summarized here; for the details the reader may consult *Singh et al.* [1996] or *Witasse et al.* [1999].The direct processes involve the ionization of atmospheric constituents by solar photons, producing photoelectrons whose impact excites metastable states. These metastable species undergo photochemistry leading to airglow emissions. For example, the $N_2(^3\Sigma_u^+)$ state is excited this way, which then collides with atomic oxygen, transferring its energy to produce excited O($^1$S). Another process is photoelectron impact on atomic oxygen. Solar UV radiation in the Schuman-Runge continuum dissociates molecular oxygen in the upper atmosphere into oxygen atoms. These atoms recombine in the three-body process $O + O + M \rightarrow O_2^* + O$, with

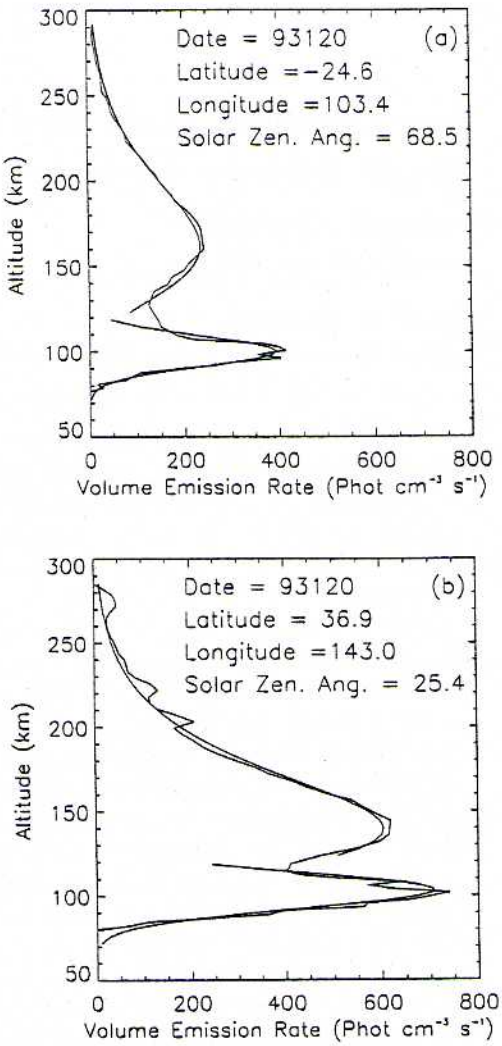


**Figure 1.** Two daytime volume emission rate profiles for 30 April 1993: (a) Solar zenith angle of 68.5° and (b) solar zenith angle of 25.4°. The jagged lines correspond to the data and the smoothed curves to their fits.

the excess energy exciting metastable $O_2^*$, which energy transfers to O to produce O($^1$S). The first step of this process is slow at 100 km so that atomic oxygen has a lifetime of days or weeks – and since it persists throughout the night it exists here in both daytime and nighttime. This is an indirect process because of the time delay between the original dissociation flux and the ultimate emission. The F region process $O_2^+ + e \rightarrow O(^1S) + O + e$ is also indirect, where the ions are originally produced through solar radiation, but have long lifetimes.

[6] Figures 1a and 1b show typical volume emission rate profiles for the 557.7 nm emission obtained in the daytime on 30 April 1993. The observed green line profiles were fitted to a Gaussian profile

$$V^g = V^g_{max} \exp -[2(h - h_{max})/w]^2 \quad (1)$$

in the E region [*Maharaj-Sharma*, 2002] and a Chapman function [*Ratcliffe*, 1972]

$$V^c = V^c_{max} \exp\left[1 - b - e^{(-b)}\right] \text{ where } b = (h - h_{max})/H \quad (2)$$

**Table 1.** Sample of E and F Region Extracted Profile Parameters

| | | Gaussian Parameters | | | Chapman Parameters | | | | | | | |
|---|---|---|---|---|---|---|---|---|---|---|---|---|
| UARS Day | Meas Number | $V^g_{max}$ Photon, $cm^{-3}$ $s^{-1}$ | $h^g$, km | w, km | $V^c_{max}$, photon $cm^{-3}$ $s^{-1}$ | $h^c$, km | H, km | Loc. Time, hrs | $\chi$ deg | Lat, deg | Long, deg | UT, hrs |
| 604 | 10 | 442 | 101.2 | 30.2 | 314 | 151.5 | 33.6 | 7.8 | 58.4 | 17.9 | 115.9 | 0.18 |
| 604 | 11 | 501 | 101.0 | 27.8 | 333 | 150.3 | 32.9 | 8.0 | 55.9 | 21.4 | 117.8 | 0.19 |
| 604 | 12 | 519 | 100.7 | 28.4 | 366 | 148.6 | 31.6 | 8.1 | 53.7 | 24.7 | 119.8 | 0.21 |
| 604 | 13 | 557 | 100.6 | 26.7 | 372 | 148.2 | 31.6 | 8.3 | 51.6 | 28.1 | 121.8 | 0.23 |
| 604 | 14 | 578 | 100.8 | 27.8 | 397 | 149.1 | 30.0 | 8.4 | 49.7 | 31.5 | 123.9 | 0.25 |
| 604 | 15 | 585 | 100.6 | 27.5 | 447 | 145.5 | 27.6 | 8.8 | 46.9 | 39.7 | 129.5 | 0.29 |
| 604 | 16 | 584 | 100.1 | 28.9 | 441 | 145.4 | 28.3 | 9.0 | 45.5 | 41.5 | 131.0 | 0.30 |
| 604 | 17 | 563 | 101.0 | 30.9 | 452 | 145.9 | 26.6 | 9.2 | 44.6 | 44.8 | 133.7 | 0.32 |
| 604 | 18 | 599 | 100.8 | 26.9 | 446 | 145.2 | 26.6 | 9.4 | 44.0 | 47.9 | 136.8 | 0.34 |
| 604 | 19 | 562 | 100.3 | 31.0 | 431 | 144.6 | 27.5 | 9.7 | 43.8 | 51.0 | 140.2 | 0.36 |
| 604 | 20 | 558 | 100.2 | 29.1 | 425 | 146.4 | 26.0 | 9.9 | 43.9 | 54.1 | 144.0 | 0.37 |
| 604 | 21 | 559 | 100.4 | 27.3 | 423 | 146.7 | 25.6 | 10.3 | 44.3 | 57.0 | 148.4 | 0.39 |

in the F region. In these expressions $V^g$ and $V^c$ are used to designate the volume emission rates of the Gaussian and Chapman functions respectively, h is the corresponding altitude, $h_{max}$ the altitude of peak emission, H is the scale height of the Chapman function and w describes the profile width of the Gaussian function. The IDL curve fitting procedure CURVFIT was used to do the fitting. The Chapman function fits the F region emission remarkably well from 130 to 300 km. The E region emission is reasonably well fitted with a Gaussian function, but there is sometimes structure as can be seen in Figure 1b, which makes it difficult to define an unambiguous peak value.

[7] The profiles show a characteristic middle thermospheric peak near 150 km (F region), corresponding primarily to processes driven by the absorption of solar EUV radiation as described above. The importance of the solar zenith angle $\chi$ may be noted; the angle measured from the local vertical at the volume of the atmosphere viewed by WINDII to the line from this volume to the sun. Figure 1a is for a larger solar zenith angle ($\chi = 68.5°$ in the figure) than in Figure 1b where $\chi = 25.4°$ and hence 1a displays smaller volume emission rates ($V^g$, $V^c$) by almost a factor of two. The altitude of the F region peak is also affected, in Figure 1a it is near 165 km, while in 1b it is a little below 150 km. Each profile fitted with CURVFIT returned six parameters; three of which describe the Gaussian component of the profile and three that describe the Chapman component. Table 1 shows a portion of the data file resulting from the CURVFIT procedure for the fitting of twelve profiles obtained on UARS day 604.

[8] Profiles of the nighttime emission are shown in Figure 2, for two different latitudes on the same day as for Figure 1. Figure 2a is for tropical latitudes (−30.4°), where the E region emission rate is relatively strong, near 300 photon $cm^{-3}$ $s^{-1}$, not so much less than in Figure 1a. In Figure 2b the latitude is 5.5° and the emission peak is very much weaker than in the daytime, at 70 photon $cm^{-3}$ $s^{-1}$. At this magnetic (APEX) latitude of 14.5° there is significant F region emission, in association with the tropical arcs of the Appleton anomaly, while in Figure 2a this emission is not discernable. Comparing Figures 1 and 2, the F region emission is overwhelmingly stronger in the daytime than at night, but this result is as expected because of the many daytime processes existing there. For the E region the daytime emission for small zenith angle is anywhere from three to ten times stronger than at night, but the reasons for this are far from obvious since the three-body recombination of O is the only mechanism that is proven to be involved.

[9] The dependence on solar zenith angle has already been noted; in Figure 3a the peak volume emission rates

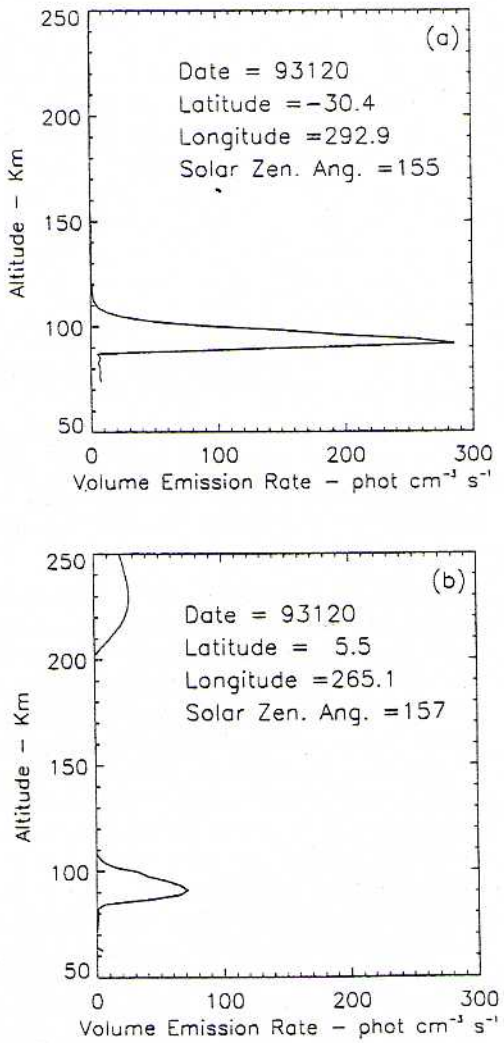


**Figure 2.** Atomic oxygen O($^1$S) nightglow profiles for 30 April 1993: (a) Latitude of 30.4°S, and (b) latitude of 5.5°N geographic, 14.5° magnetic.

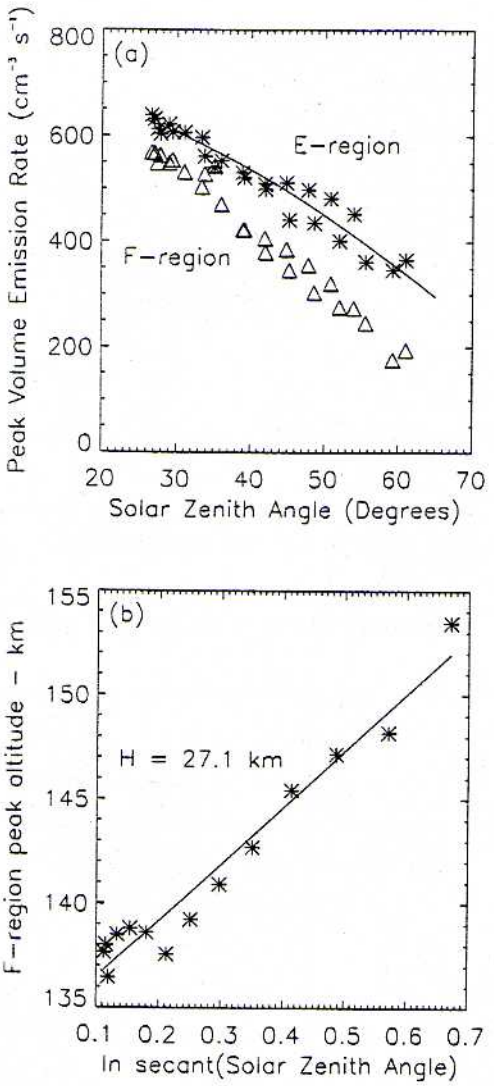


**Figure 3.** (a) Peak volume emission rate versus solar zenith angle for 28 January 1995 for E and F regions and (b) plot of the altitude of the F region emission peak versus ln sec($\chi$) for the same day. The solid lines are fits to the data.

$V^g_{max}$ and $V^c_{max}$ for the E and F regions respectively are plotted for a portion of one orbit on Jan. 28, 1995 versus solar zenith angle, and a highly systematic correlation is obvious. The E region data are fitted with a cos $\chi$ function, which represent the data very well. The same function would not as closely fit the F region curve. The cos $\chi$ relationship is expected from the Chapman equation [*Ratcliffe*, 1972] for the approximation of a flat earth. The reason for this F region departure was not identified, but may relate to the higher altitude thickness of the emitting region. The Chapman [illegible] very strongly suggests that as in the F region, [illegible] is dominantly produced by a direct process, in addition to the E region atomic oxygen recombination that solely produces the emission at night. There is another test of the applicability of the Chapman equation, through the following equation obtained in its derivation:

$$h_{max} = H \ln(\sigma\, n_o\, H) + H \ln(\sec \chi) \qquad (3)$$

where H is the scale height, $\sigma$ is the absorption cross section, $n_o$ is the number density at the reference altitude and $h_{max}$ is the altitude of the emission peak. The observed data can be tested for Chapman-like behavior by plotting $h_{max}$ versus ln (sec $\chi$); the slope yields H and the intercept then provides a value of $\sigma\, n_o$.

[10] In Figure 3b the peak altitude for the F region $h^c_{max}$ is plotted versus ln (sec $\chi$) for the same day and a very strong correlation is found, with a correlation coefficient of 0.98 and a well-defined slope of 27.1 km, similar to values of the scale height found in the Chapman fit and shown in Table 1. For the E region, inconsistent results were found. There are some good reasons for this. The height variation here is very small, a few km, and the measurement accuracy is only about 0.75 km. More importantly, dynamical influences have a drastic effect on the altitude of the nightglow emission [*Shepherd et al.*,1995; *Zhang et al.*, 2001], both through tides and planetary waves. To obtain a plot as in Figure 3b for a single day, the emission rates for different $\chi$ values come from different latitudes, longitudes and local times, with consequent different dynamical forcing. To obtain such a plot for a single latitude would require sampling data over six months, which would create other problems. However, information about the absorption cross section is provided simply by the peak altitude, estimated at 105 km for overhead sun. Setting the reference altitude at the layer peak for an overhead sun corresponds to $h_{max} = 0$ and sec $\chi = 1$, so that one obtains $\sigma = 1/(n_o H)$, and using MSIS-90 values of $n_o$ and H the value $\sigma = 2.3 \times 10^{-18}$ cm$^2$ results. This is close to the absorption cross section of $2.2 \times 10^{-18}$ cm$^2$ for the photo-dissociation of $O_2$ at 102.6 nm, the wavelength for Lyman-$\beta$, as obtained by *Holland et al.* [1993]. This is consistent with the process suggested by Richard Link, $h\nu + O_2 \rightarrow O(^1S) + O$, where the $h\nu$ photon corresponds to Lyman-$\beta$. To make the deduced cross section equal to the actual one at 102.6 nm it is necessary only to change the peak altitude to 103 km, which is reasonable. Thus the peak altitude is fully consistent with the absorption of 102.6 nm solar radiation by $O_2$. The peak volume emission rate is given by another step in the Chapman equation derivation:

$$V_{max} = q\, I/(e\, H \sec \chi) \qquad (4)$$

where e is the base of natural logarithms, I is the solar irradiance and q is the yield for the production of $O(^1S)$ in a dissociation; neither the cross section nor the number density appear in this equation. A value of $2 \times 10^{-4}$ W m$^{-2}$ nm$^{-1}$ was obtained from the daily spectrum on the SEE (TIMED) website for June 2003 (a review of recent SEE results is given by *Woods et al.* [2003]). For overhead sun and a bandwidth of 1 nm (the SEE resolution element) the resulting value for $V_{max}$ is 777 photon cm$^{-3}$ s$^{-1}$. This is very close to the peak volume emission rate shown in [illegible] 1b for $\chi = 25.4°$, with the sun almost overhead, but going back one solar cycle from June 2003 corresponds to mid 1992, for which the emission rate is a little higher, as shown in Figure 5, where 500 photon cm$^{-3}$ s$^{-1}$ is appropriate for 60° solar zenith angle, or 1000 photon cm$^{-3}$ s$^{-1}$ for overhead sun. To the estimated 777 photon cm$^{-3}$ s$^{-1}$ the atomic oxygen recombination component needs to be added, perhaps 100 photon cm$^{-3}$ s$^{-1}$, but as well there is additional

Table 2. Wavelength Ranges and Source Regions for the Solar Indices

| Spectral Region | Solar Index | Wavelength Range | Source Region |
|---|---|---|---|
| Short-wave X-ray | GOES (xs) | 0.05–0.4 nm | Corona |
| Long-wave X-ray | GOES (xl) | 0.1–0.8 nm | Corona |
| Longer-wave X-ray | YOHKOH | 0.8–2.0 nm | Corona |
| Far ultraviolet | Lyman-α | 121.6 nm | Chromosphere |
| Near ultraviolet | MgII | 280.0 nm | Chromosphere |
| Near infra-red | HeI Index | 1083.0 nm | Chromosphere/Corona |
| Radio | F10.7 cm | $10.7 \times 10^7$ nm | Chromosphere/Corona |

irradiance in the vicinity of the Lyman-β line. This line is a factor of ten above background, and the O($^1$S) yield peaks near 106 nm at about 0.1, falling sharply at longer wavelengths according to *Lawrence and McEwan* [1973]; this limits the contribution of the irradiance outside Lyman-β. Thus there is some predicted over-production of the O($^1$S) emission, giving some confidence to the conclusion for the process, given the uncertainties, particularly in the O($^1$S) yield. A more detailed modeling analysis will be undertaken in a separate work, but for now it appears that Lyman-β is the dominant source.

## 3. Solar Indices and the Solar Dataset

[11] To evaluate the solar influence on atomic oxygen green line daytime emission and its variability, a set of solar indices was chosen from the x-ray, ultraviolet and radio regions of the electromagnetic spectrum for correlation with the green line emission. A list of the wavelength regions, their corresponding solar source regions, and the solar indices that relate to them is given in Table 2.

[12] Six solar indices were used for the present study, HeI, Lyman-α, F10.7, MgII, YOHKOH and GOES. The HeI index is provided by the Kitt Peak Vacuum Telescope that obtains full-disk images of the Sun by scanning the solar image across a long-slit spectrograph. One of the five images obtained is the equivalent width of the helium 1083 nm solar absorption line in units of milliAngstroms, averaged over the solar disk. This absorption line is believed to originate almost entirely in the chromosphere, with some contribution from the chromosphere-corona transition region and the solar corona. The Lyman-α index is the irradiance corresponding to this emission line at 121.6 nm, in W m$^{-2}$. This line is measured by both the SOLSTICE and SUSIM instruments on the Upper Atmosphere Research Satellite (UARS), so clearly covers the WINDII period of observations; a model for this irradiance was presented by *Woods et al.* [2000]. It is emitted from a wide range of heights in the chromosphere. The F10.7 index comes from a radio emission of 10.7 cm wavelength. Radio flux levels consist of emission from three sources: from undisturbed solar quiet regions, from developing active regions and from short-lived enhancements above daily levels. Solar irradiance at 2800 MHz (F10.7 cm) was recorded routinely by a radio telescope near Ottawa between 1947 and 1991 [*Tapping*, 1987] and since June 1991, the radio telescope has been located at Penticton, British Columbia, Canada. The 10.7 cm solar flux is given in solar flux units (1 sfu = $10^{-22}$ W m$^{-2}$ Hz$^{-1}$).

[13] The broad Mg II absorption feature in the solar UV spectrum is centered at a wavelength of about 279.9 nm. It is the result of the overlap of two Mg II absorption lines in the solar irradiance from the sun's photosphere. By contrast, the two Mg II emission lines located at the base of this composite feature originate from higher in the solar atmosphere in the chromosphere. The behavior of these lines' irradiance through time has been found to be a convenient proxy for changes in chromospheric and upper photospheric UV flux at other wavelengths. Generally described, the Mg II index is the ratio of the irradiance at the core of the Mg II feature (containing the variable emission lines) to that of its relatively less variable wings.

[14] The YOHKOH satellite is a Japanese observatory for studying x-rays and gamma rays from the sun, launched on 31 August 1991, with contributions from both the U.S. and the U.K. The spacecraft carries a payload of four scientific instruments, one of which is the Soft X-ray Telescope (SXT) used for the measurements described here. The SXT, which is sensitive in the range 0.1–5 nm, takes images in various wave bands (selected by filters) using a CCD. The YOHKOH data used in this work were from the SXT, for the wavelength band 0.8–2.0 nm and were kindly provided by Loren Acton. This index is simply the irradiance in W m$^{-2}$; the derivation of the irradiance from the observations is described by *Acton et al.* [1999].

[15] The x-ray spectrum below 1 nm is characterized by its steepness and its extreme variability. Measurements are provided by the NOAA Geosychronous Operational Environmental Satellites (GOES). Amongst other measurements, GOES monitors solar x-ray fluxes at geostationary orbit. Ion-chamber detectors provide whole-sun x-ray fluxes for the 0.1 to 0.8 nm (xl) and the 0.05 to 0.4 nm (xs) wavelength bands; the data from the xl channel are used here. The x-ray emission of the sun is determined once during each spin for a spin period of 0.6 seconds and the data for both bands are given in Watt m$^{-2}$. The GOES fluxes used for the daily correlations of this work are daily averages obtained from the GOES website for the period studied.

[16] The plots shown in Figures 4a–4f present the time series variation of these six solar indices over the period 17 January 1993 to 23 March 1995. The calendar dates are shown at the top of each figure, the added ticks indicate 1 January for each year. Both the HeI and the Lyman-α indices show an almost 50% decrease over the period January 1993 to March 1995, while the F10.7 and the MgII indices decay by about 77% and 12% respectively. The YOHKOH irradiance shows an overwhelming 88% decrease because its value at solar maximum is near zero, unlike the other indices. The GOES xl irradiance is completely different. It shows an almost random behavior with no evident dependence on the solar cycle.

[17] In Figure 4 all the different solar indices, other than the GOES x-rays, have the same general behavior with time, which is a little surprising considering that they are associated with different solar regions. The Ly-α irradiance is different in detail in that its pattern does not show the spikes around UARS days 400, 600 and 850 that are evident for the other indices, and as noted, the GOES xl x-rays are highly sporadic.

## 4. Greenline Data

[18] To meaningfully interpret the planned correlations it was necessary that daily values for the green line volume

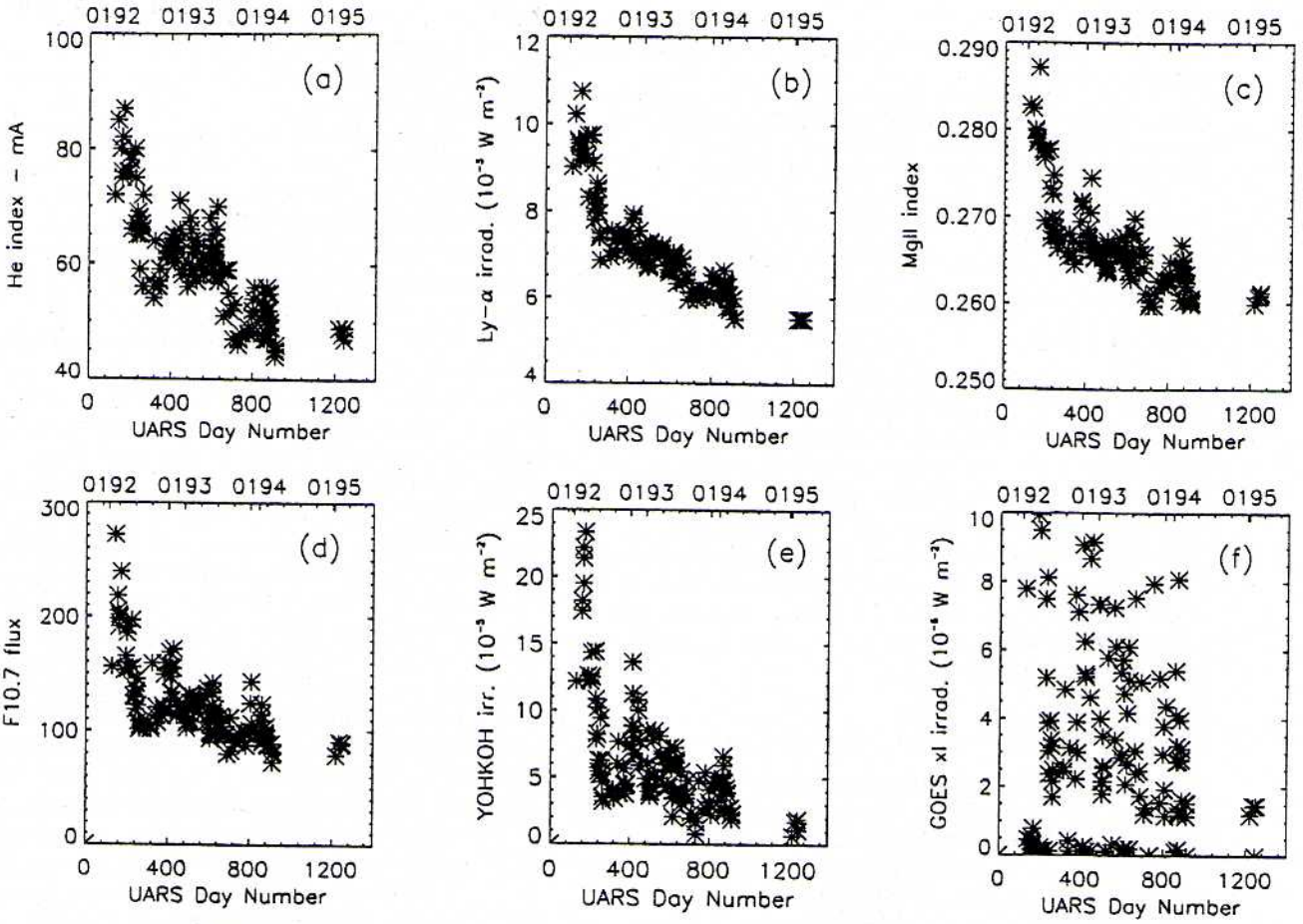


**Figure 4.** Time series variation for six solar indices: (a) HeI, (b) Lyman-α, (c) MgII, (d) F10.7 cm, (e) YOHKOH, and (f) GOES xl. The UARS day numbers are shown below, and the calendar dates above.

emission rates be generated for comparison with the solar indices. Although several hundred dayglow emission profile are obtained on a single day they cannot all be averaged together because each has a different solar zenith angle, and the distribution of these varies from day to day because the local time (LT) for WINDII advances by 20 minutes for each successive day, and it varies with latitude, with the smallest value of $\chi$ (the sun closest to overhead) occurring near the equator. When the local time is near twilight at the equator, the sun will never be high in the sky, so small $\chi$ values are never observed, but there will always be a sunrise and sunset, so it was decided to use a solar zenith angle of 60° for the daily value. Then when the equatorial local time is near noon, $\chi$ is small near the equator, but must cross 60° before it reaches the terminator. So a $\chi$ of 60° is observed on almost every day. For this reason the daily averaged value of emission rate was calculated by averaging all profiles measured at a $\chi$ of 6[illegible]ure 3a it may be noted that each plot has two b[illegible] from the morning period (AM) and the other for the [illegible] in the afternoon (PM). Therefore the AM and PM val[illegible] treated separately. The procedure adopted to determine [illegible] daily value of greenline volume emission rate was:

[19] 1. Identify all dayglow profiles measured with $59.5 < \chi < 60.5$, separating the AM profiles (those measured before 12:00 LT) from the PM profiles.

[20] 2. For each day, average all the E region maxima of the AM and PM profiles to give daily averaged $V^g_{max}$ values for AM and PM.

[21] 3. For each day, average all the F region maxima of the AM and PM profiles to give a daily averaged $V^c_{max}$ values for the AM and PM.

[22] In Figure 5 the time variation of the E region AM emission is shown in a and the F region variation for the AM emission is shown in b. The variation is similar to that of the solar indices HeI, Ly-α, Mg-II and F 10.7 for the E region, but the F region shows more scatter, likely because of the indirect processes involved.

[23] The AM and PM daily averages for both the E and F regions were separately correlated with the daily values of each of the solar indices. Figures 6 to 11 show these correlations. Table 3 shows the correlation coefficients derived for the solar indices for both the E and F regions and both AM and PM local times. From this table it is seen that the correlation coefficients for the E region are always higher than for the F region. For both regions, the AM correlation coefficients are higher than for the PM, suggesting that the direct processes have less influence in the afternoon, perhaps because of the buildup of ionization, or atomic oxygen. This would appear to contradict the fact that the peak emission rates are higher in the AM than in the PM, as seen in Figures 6–10, especially for the F region.

However, the AM/PM differences are not that large, and for a 57° orbit there is a strong coupling of local time to latitude, making it impossible to be definitive about the origin of these differences. The highest value of correlation coefficient was obtained for the Lyman-α index, which suggests that this index is the one most closely related to the green line variability. The generally lower correlation coefficients found for the F region may result from the number of different processes involved, some of which are indirect. In the E region the atomic oxygen recombination process is indirect, so the high correlation strongly supports the earlier conclusion that the largest component of the daytime emission is produced by direct excitation, mainly by Lyman-β. Since Lyman-β irradiance is expected to be proportional to that of Lyman-α the high correlation with the latter is consistent with this conclusion.

[24] The GOES xl x-rays depicted in Figure 11 show no correlation at all, which is consistent with their seemingly random behavior shown in Figure 4f, but this can be explained simply by the difference in irradiance levels.

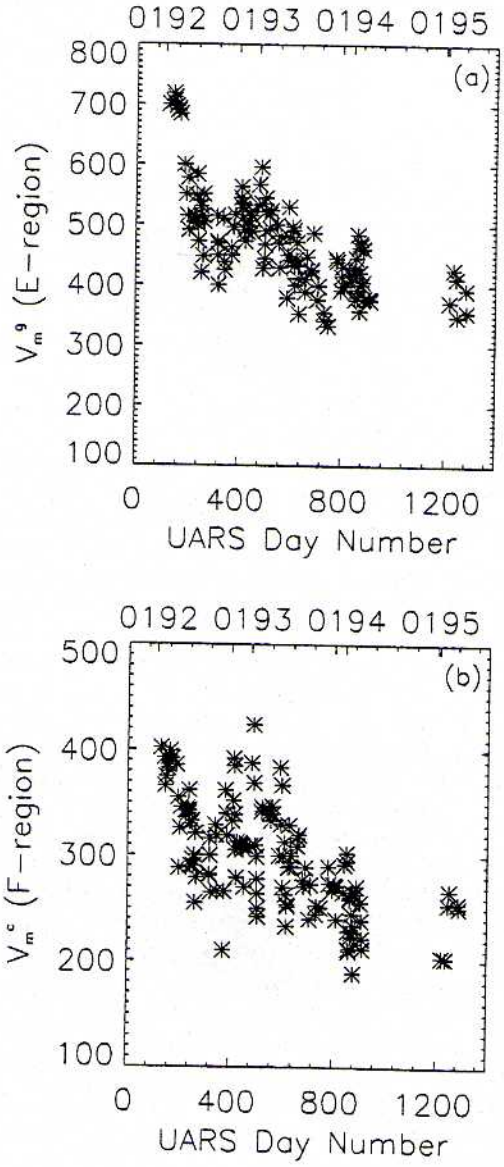


**Figure 5.** Time series variation of the peak O($^1$S) daytime emissions (a) for the E region and (b) for the F region. UARS day numbers are shown below, and the calendar dates for January 1 are shown above.

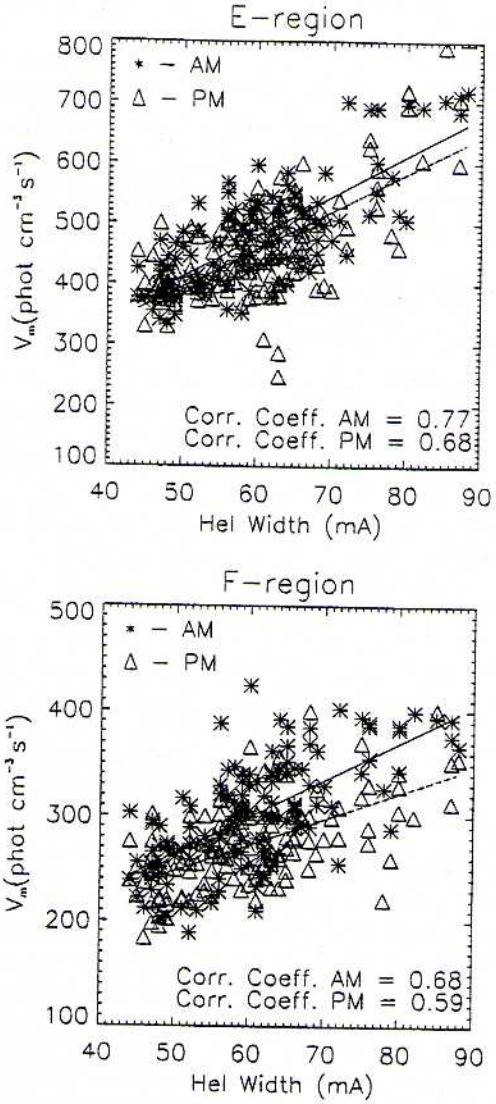


**Figure 6.** Correlation of peak volume emission rate with HeI width: (a) E region and (b) F region. The solid lines are linear fits to the data, and the correlation coefficients are shown.

**Table 3.** Correlation Coefficients of Solar Indices with Greenline Volume Emission Rates

| Solar Index | E Region (AM) | E Region (PM) | F Region (AM) | F Region (PM) |
|---|---|---|---|---|
| HeI | 0.77 | 0.68 | 0.68 | 0.59 |
| Lyman-α | 0.82 | 0.73 | 0.66 | 0.59 |
| YOHKOH | 0.71 | 0.70 | 0.66 | 0.57 |
| Mg-II | 0.78 | 0.70 | 0.67 | 0.62 |
| F-10.7 | 0.77 | 0.72 | 0.61 | 0.55 |
| GOES xl | 0.01 | −0.07 | 0.07 | 0.05 |

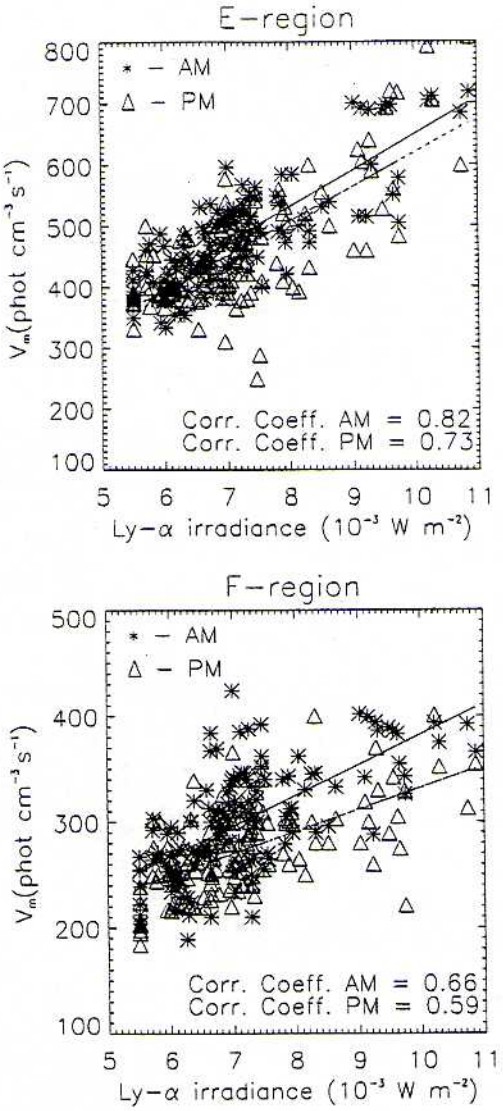


**Figure 7.** Correlation of peak volume emission rate with Lyman-α irradiance: (a) E region and (b) F region. The solid lines are linear fits to the data, and the correlation coefficients are shown.

For the YOHKOH x-rays in Figure 4e the maximum irradiance is $25 \times 10^{-5}$ W m$^{-2}$, while for the GOES xl x-rays it is $10 \times 10^{-6}$ W m$^{-2}$, a factor of 25 lower, which clearly does not produce observable emission. Thus there are two remarkable differences between the GOES xl wavelength range of 0.1–0.8 and the YOHKOH range of 0.8–2.0 nm, the large difference in irradiance that is consistent with an extremely steep spectrum, and the very different responses to the solar cycle.

[25] What can be learned from these six correlations? For the E region AM, the correlation coefficient is 0.82 for Ly-α, closely followed by Mg-II, HeI and F10.7, with coefficients of 0.78 or 0.77. It is remarkable that these coefficients are so similar, considering the different solar regions from which they come, and their nature. The Mg-II and HeI indices are measures of line depths and widths, and have no direct relationship with the irradiances that excite the green line; they are proxies for those EUV radiances that produce the F region green line emission, and so it would seem also for the Ly β that produces the E region emission. The Ly α emission cannot produce the green line, but since it is proportional to the Ly β emission which does so, it appears to be a kind of "direct proxy" of E region green line emission, and a normal proxy for the F region. The F10.7 index is a radio irradiance, but it cannot excite the green line; it too is a proxy. While the YOHKOH 0.8–2.0 nm irradiance can potentially excite the green line it has a significantly lower correlation coefficient of 0.71 than the four indices discussed above. From the available information it is not possible to determine the extent to which the YOHKOH x-rays are directly responsible for the production of green line emission. The GOES xl x-rays are also potential excitation sources, but their radiances levels are ordinarily too low to produce green line emission; they are greatly enhanced during solar flares, when green line emission is also enhanced, so may

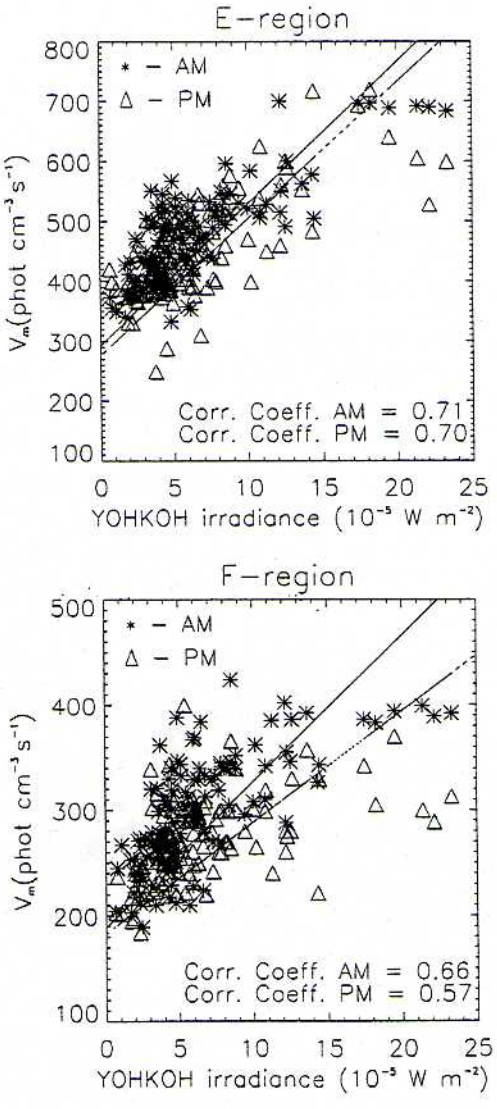


**Figure 8.** Correlation of peak volume emission rate with YOHKOH irradiance: (a) E region and (b) F region. The solid lines are linear fits to the data, and the correlation coefficients are shown.

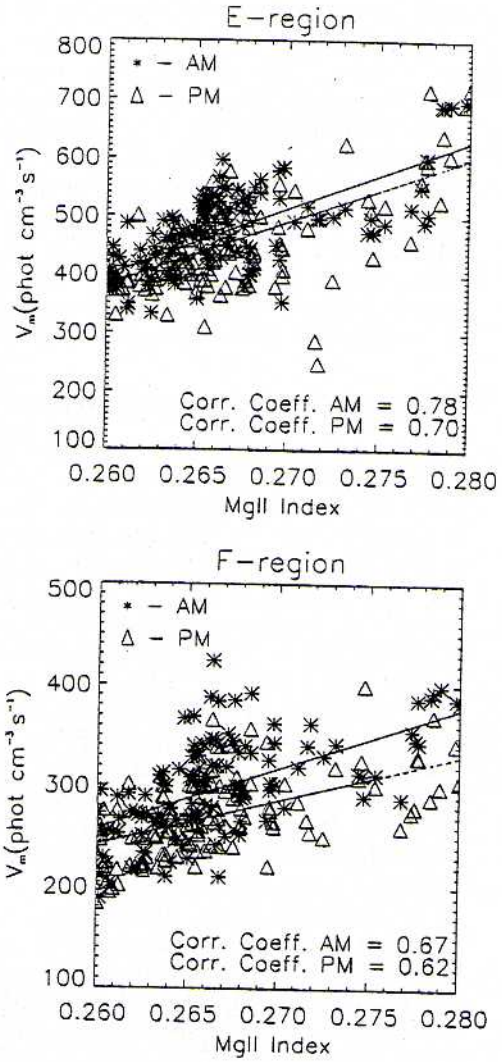


**Figure 9.** Correlation of peak volume emission rate with MgII index: (a) E region and (b) F region. The solid lines are linear fits to the data, and the correlation coefficients are shown.

then be a direct source. That topic is the subject of a future publication.

## 5. Atomic Oxygen Recombination Contribution

[26] The high correlation coefficients found for five of the six solar indices with the E region green line is puzzling, because the atomic oxygen recombination process must still play a significant role in the daytime. To a first approximation, this contribution would be the same in the daytime as at night. With this assumption, subtracting the night-glow emission component from the dayglow emissions would leave only the daytime component produced by direct excitation. When this was done, and the "corrected" direct green line dayglow emissions were correlated with the Lyman- $\alpha$ solar index the correlation coefficient was reduced from 0.81 to 0.80. This suggests that the nighttime recombination of atomic oxygen makes a rather small contribution to daytime variability, or alternatively that dynamical influences on atomic oxygen concentration make the daytime values totally uncorrelated with the nighttime values. The tidal influence on atomic oxygen is significant, as has been observed for the night airglow with WINDII as described by *Shepherd et al.* [1997b], *Zhang et al.* [2001] and *Ward* [1999].

## 6. Latitudinal and Longitudinal Variations

[27] The green line emission rate depends not only on the solar flux, but also on the atmosphere, so that variations in atmospheric total density, or in composition have some influence on the emission rates, and thus on the correlations. To explore the possible influence of this atmospheric variability, correlations between daytime green line volume emission rates (E and F regions) and the Lyman-$\alpha$ solar index in the tropical (−20.0–20.0) and mid (20.0–50.0; −20.0–(−50.0)) latitude bands were compared. The results

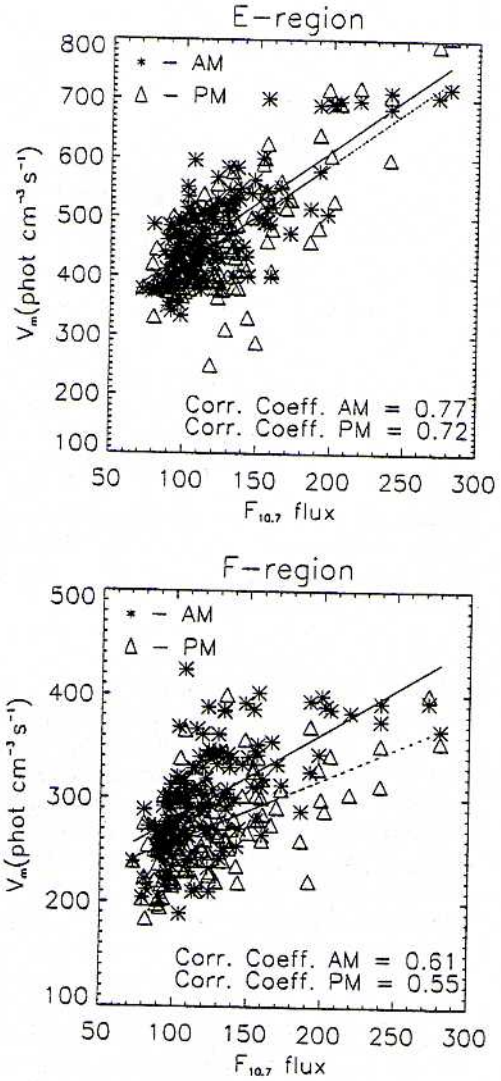


**Figure 10.** Correlation of peak volume emission rate with F10.7 cm flux: (a) E region and (b) F region. The solid lines are linear fits to the data, and the correlation coefficients are shown.

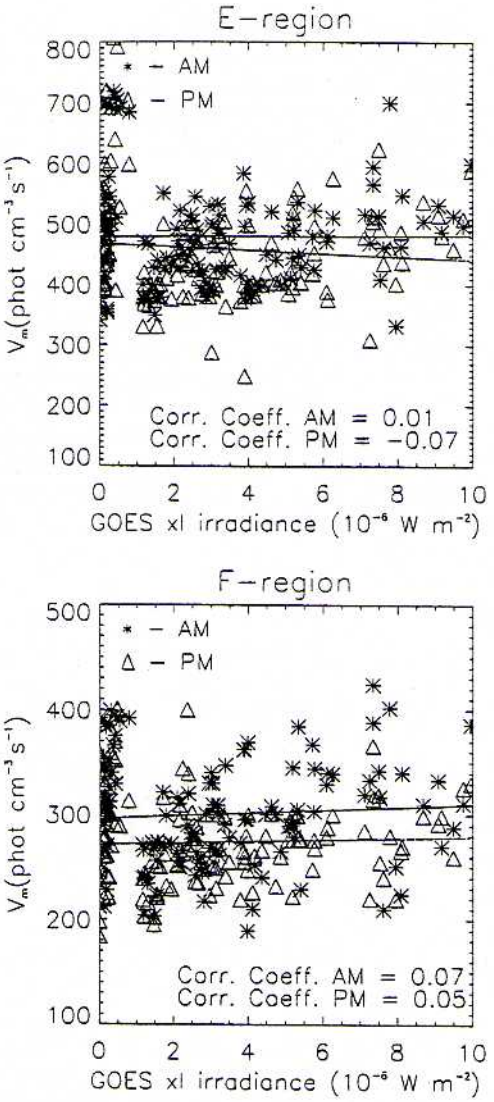


**Figure 11.** Correlation of peak volume emission rate with GOES xl x-rays: (a) E region and (b) F region. The solid lines are linear fits to the data, and the correlation coefficients are shown.

indicated that there was no evidence of a noticable general latitudinal dependence on green line correlations. It is not possible to make detailed comparisons because for the same day, different latitudes correspond to different local times and it is not really possible to separate latitude from the AM/PM (local time) differences discussed earlier.

[28] A longitudinal variation for WINDII night airglow emission was reported by *Shepherd et al.* [1993b], and interpreted as planetary waves. High latitude planetary wave structures were described by *Shepherd et al.* [1999] in association with a stratospheric warming, again at night. In the context of this study, the question is as to whether planetary scale disturbances produce emission rate variations in the daytime, under the influence of direct excitation of O($^1$S). Figure 12 shows the longitudinal variation of emission rate for both the E and F regions for 28 January 1993, for a fixed solar zenith angle of 60°. For a single day, the same solar zenith angle occurs at the same latitude, which in this case is −34°. Variation is evident in both regions, resembling wave 2, with a phase shift between E and F regions. The jump at 240° longitude, where two points appear at almost the same longitude marks the change from one day to the next; this discontinuity indicates the day-to-day change. The data from 15 January to 30 January 1993 were investigated, and the planetary wave structure was found to move slowly, and gradually change pattern from day to day. *Ward et al.* [1997] found similar emission rate variations in the 2-day wave at night; it seems reasonable that this influence should exist in the daytime as well even though the excitation mechanisms are different.

## 7. F-Region Scale Height Variations

[29] As seen in Figure 1, the F region green line emission is remarkably well fitted by a Chapman function, raising the question as to the meaning of the associated scale height. In the Chapman function derivation the scale height is that of the absorbing species, but the scale height observed here is that of the excited O($^1$S), which depends on the excitation processes involved, as well as the diffusive equilibrium of atmospheric species involved. For diffusive equilibrium, the temperature is calculated simply from T = mgH/k, where m is the species mass, g the acceleration of gravity, k the Boltzman constant, and T the temperature. Adopting this relation, and assuming atomic oxygen to be the species associated with the scale height, the temperature corresponding to each scale height was calculated for each day, for the restricted latitude band 30°−40° north and south latitude. A time series plot of WINDII "temperature" for the period studied in this work is presented in Figure 13a. For comparison, the temperature time series profile for the MSIS-90 model at an altitude of 140 km is shown in Figure 13b. It is seen that while the WINDII temperatures are slightly higher, the response to the solar cycle variation is similar for both WINDII and MSIS-90. The main difference is that the WINDII data show larger short term variability, which is not reflected in the model. The altitude of 140 km is effectively at the base of the Chapman layer. Thus the WINDII Chapman-layer scale heights appear to

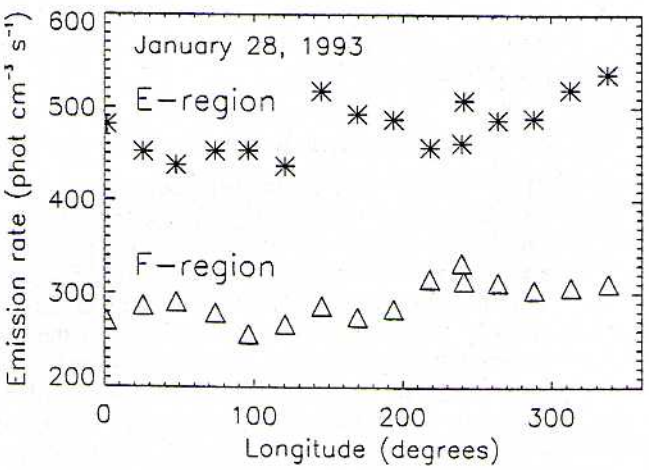


**Figure 12.** Longitudinal variation of peak volume emission rate for the E and F regions on 28 January 1993, for a solar zenith angle of 60° and a latitude of 34°S.

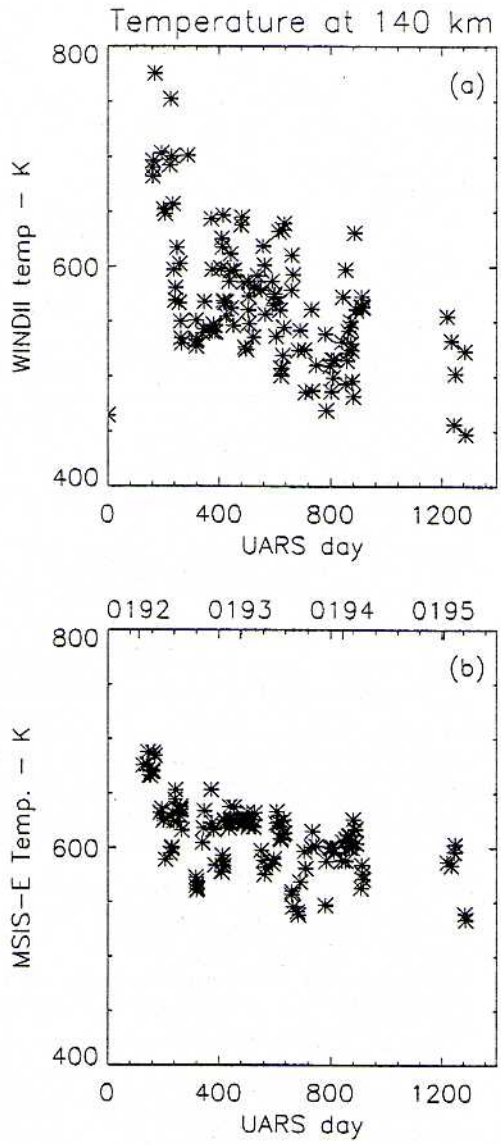


**Figure 13.** (a) Plot of temperature derived from green line F region scale height versus UARS day; (b) plot of MSIS-90 temperature at 140 km versus UARS day, with calendar dates shown above.

provide some information about the temperature at its base. More detailed modeling is needed to better understand why this scale height is so well-defined considering the actual variations of temperature and photochemical processes involved over this altitude range. As well, further work is needed to determine whether the short-term temperature variations are real or not.

## 8. Discussion and Conclusions

[30] This study is concerned with a unique data set, the WINDII daytime green line O($^1$S) emission rate profiles. This profile comprises two distinct regions, one in the middle thermosphere called herein the F region and another in the lower thermosphere herein referred to as the E region. The excitation processes involved in these two regions are completely different. Those for the F region have been well-studied and it can be said that they are rather fully understood, as described above. The E region emission at first sight resembles the narrow nighttime airglow layer near 100 km, but the peak emission is about 3 to 10 times greater than at night, and more extended in vertical extent; the excitation mechanism for this excess emission has not been previously identified. The intent of this work was to study the long-term solar variability of this emission in order to better understand the solar influence on the thermosphere, but in order to do that it is important that the mechanism be understood.

[31] Both regions showed a clear dependence of peak emission rate on cos $\chi$, and a variation of peak altitude with $\chi$ that corresponds to the Chapman function and thus direct solar excitation processes; this in spite of the fact that both regions, and especially the E region, are in part excited by indirect processes. The peak emission rates for these two emissions were correlated with six solar indices; Ly $\alpha$, HeI, MgII and F10.7 had correlation coefficients between 0.82 and 0.77 for the E region AM, with YOHKOH a little lower at 0.71. For the F region AM there was a difference in that values for Ly $\alpha$, HeI, MgII and YOHKOH were all between 0.68 and 0.66, while F10.7 was a little lower at 0.61. In summary, Ly $\alpha$ HeI and MgII have similar correlations for both the E and F regions, while YOHKOH is slightly lower for the E region and F10.7 slightly lower for the F region.

[32] One possible explanation for the lower correlations for the F region is the number and extent of the processes giving rise to green line emissions; there are fewer processes in the E region. A mechanism for the direct E region excitation has been proposed by Dr. Richard Link (private communication) as photodissociative excitation of O($^1$S) through absorption of Lyman-$\beta$ in $O_2$. The peak altitude of the E region emission yields a value of $\sigma n_o$, and knowing the number density $n_o$ for $O_2$, $\sigma$ was calculated and found to be equal to the absorption cross section of $O_2$ by Lyman-$\beta$. The Lyman-$\beta$ radiances measured by the SEE instrument on the TIMED satellite slightly over-predict the E region peak volume emission rate, using a yield of 0.1. These two pieces of evidence provide very strong evidence that Ly $\beta$, along with some additional irradiance in the same spectral region, is the source for the direct process for the daytime E region.

[33] For the statistical study a Gaussian function was used to fit the E region data, as described earlier. For the Ly $\beta$ process this should of course be a Chapman function. Limited tests of Chapman fits were made retrospectively and found to be reasonable. An accurate fitting for the E region is complicated by the presence of the atomic oxygen recombination component, so that there are really two layers – evident separately in a few profiles observed, and by the strong influence of dynamics in this region of the atmosphere.

[34] Other aspects of the correlation were studied; and all of the conclusions are summarized as follows.

[35] 1. The E and F region components of the daytime O($^1$S) emission correlate strongly with all solar indices except short wavelength x-rays when daily indices are used; the best correlation is with Ly $\alpha$, and for this the E region gives the higher value.

[36] 2. The strong daytime E region emission has not been previously observed, or explained. The altitude of the emission peak, and the peak emission rate are consistent

with photodissociation of $O_2$ by Lyman-β as the primary process.

[37] 3. Both regions show a similar dependence on solar zenith angle and for the same solar zenith angle, the morning emissions are somewhat stronger than in the afternoon, more so for the F region. However, for a given orbit the local time is directly related to latitude, so the meaning of this is not certain. The pre-noon emissions are also better correlated with the solar indices than are those for the afternoon, suggesting a greater role for the direct processes in the morning.

[38] 4. No latitudinal differences in the correlations are found, indicating that although the atmospheric characteristics must be considered along with the solar radiances, the influence appears to be small. Longitudinal planetary scale structures in the O($^1$S) emission are observed, which appear to originate from the influence of dynamics on composition, as has been observed for airglow emissions at night.

[39] 5. The scale height of the F region emission yields temperatures that correspond approximately to the base of the Chapman layer; these temperatures mimic the variations of the MSIS model but show larger day-to-day variations than are evident in the model.

[40] **Acknowledgments.** The authors are grateful to those scientists who produced the solar indices and made them so freely available. The NSO/Kitt Peak data used here (for the HeI indices) are produced cooperatively by NSF/NOAO, NASA/GSFC and NOAA/SEC. The Ly α values were obtained from the UARS database. We are grateful to Loren Acton of the University of Montana for providing the YOHKOH values as well as helpful comments. The MgII values were obtained from the Naval Research Laboratory website. The GOES data are provided by NOAA while the F10.7 cm data come from the Dominion Radio Astrophysical Observatory of the National Research Council of Canada, in Penticton, British Columbia. The Ly β data were taken from the SEE/TIMED website, in consultation with Tom Woods. We are grateful to Richard Link for suggesting the Ly β process, and for providing the numerical cross section values from *Holland et al.* [1993]. The authors also thank Brian Solheim, Ian McDade, Gary Rottman, Shengpan Zhang, Chantal Lathuillere and Frederic Culot for helpful discussions and suggestions, as well as the reviewers. The WINDII project is supported by the Canadian Space Agency and the Centre National d'Etudes Spatiales of France; the scientific data analysis is supported by the Natural Sciences and Engineering Research Council of Canada.

## References

Acton, L. W., D. C. Weston, and M. E. Bruner (1999), Deriving solar X ray irradiance from Yohkoh observations, *J. Geophys. Res.*, *104*, 14,827–14,832.

Bens, A. R., L. L. Cogger, and G. G. Shepherd (1965), Upper atmospheric temperatures from Doppler line widths - III. Observation of the OI dayglow emission at 6300 Å, *Planet. Space Sci.*, *13*, 551–563.

Chakrabarti, S. (1998), Ground based spectroscopic studies of sunlit airglow and aurora, *J. Atmos. Sol. Terr. Phys.*, *60*, 1403–1423.

Hays, P. B., G. Carignan, B. C. Kennedy, G. G. Shepherd, and J. C. G. Walker (1973), The visible airglow experiment on Atmospheric Explorer, *Radio Sci.*, *8*, 369–377.

Hedin, A. E. (1991), Extension of the MSIS thermosphere model into the middle and lower atmosphere, *J. Geophys. Res.*, *96*, 1159–1172.

Hill, S. M., S. C. Solomon, D. D. Cleary, and A. L. Broadfoot (2000), Temperature dependence of the reaction $N_2$ ($A^3\Sigma_u^+$) + O in the terrestrial atmosphere, *J. Geophys. Res.*, *105*, 10,615–10,629.

Holland, D. M. P., D. A. Shaw, S. M. McSweeney, M. A. MacDonald, A. Hopkirk, and M. A. Hayes (1993), A study of the absolute photoabsorption, photoionization and photodissociation cross sections and the photoionization quantum efficiency of oxygen from the ionization threshold to 490 Å, *Chem. Phys.*, *173*, 315–331.

Lawrence, G. M., and M. J. McEwan (1973), Production of O($^1$S) from photodissociation of $O_2$, *J. Geophys. Res.*, *78*, 8314.

Maharaj-Sharma, R. (2002), Solar variability of the atomic oxygen greenline emissions in the middle and lower thermosphere, Ph.D. Thesis, York Univ., Toronto, Can.

Noxon, J. F. (1968), Day airglow, *Space Sci. Rev.*, *8*, 92–134.

Pallamraju, D., J. Baumgardner, S. Chakrabarti, and T. R. Pedersen (2001), Simultaneous ground based observations of an auroral arc in daytime/twilighttime OI 630.0 nm emission and by incoherent scatter radar, *J. Geophys. Res.*, *106*, 5543–5549.

Ratcliffe, J. A. (1972), *An Introduction to the Ionosphere and Magnetosphere*, Cambridge Univ. Press, New York.

Shepherd, G. G. (2002), *Spectral Imaging of the Atmosphere*, Academic,-San Diego, Calif.

Shepherd, G. G., et al. (1993a), WINDII, The Wind Imaging Interferometer on the Upper Atmosphere Research Satellite, *J. Geophys. Res.*, *98*, 10,725–10,750.

Shepherd, G. G., et al. (1993b), Longitudinal structure in atomic oxygen concentration observed with WINDII on board UARS, *Geophys. Res. Lett.*, *20*, 1303–1306.

Shepherd, G. G., C. McLandress, and B. H. Solheim (1995), Tidal influence on O($^1$S) airglow emission rate distribution at the geographic equator as observed by WINDII, *Geophys. Res. Lett.*, *22*, 275–278.

Shepherd, G. G., N. J. Siddiqi, R. H. Wiens, and S. Zhang (1997a), Airglow measurements of possible changes in the ionosphere and middle atmosphere, *Adv. Space Res.*, *20*, 2127–2135.

Shepherd, G. G., R. G. Roble, C. McLandress, and W. E. Ward (1997b), WINDII observations of the 558 nm emissions in the lower thermosphere: The influence of dynamics on composition, *J. Atmos. Sol. Terr. Phys.*, *59*, 655–667.

Shepherd, G. G., S. Zhang, and X. Wang (1999), Variability in MLT dynamics and species concentrations as observed by WINDII, *Earth Planets Space*, *51*, 845–853.

Siddiqi, N. J. (1996), Solar variation of the oxygen greenline nightglow, M. Sc. Thesis, York Univ., Ontario, Can.

Singh, V., and S. Tyagi (2002), Testing of solar EUV flux models using 5557 Å, 6300 Å and 7320 Å dayglow emissions, *Adv. Space Res.*, *30*, 2557–2562.

Singh, V., I. C. McDade, G. G. Shepherd, B. H. Solheim, and W. E. Ward (1996), The O($^1$S) dayglow emission as observed by the WIND Imaging Interferometer on the UARS, *Ann. Geophys.*, *14*, 637–646.

Sridharan, R., A. Taori, S. Gurubaran, R. Rajaram, and M. G. Shepherd (1999), First results on daytime mesopause OH rotational temperatures using ground-based photometry from equatorial latitudes, *J. Atmos. Sol. Terr. Phys.*, *61*, 1131–1142.

Taori, A., R. Sridharan, D. Chakrabarty, N. K. Modi, and R. Narayanan (2003), Significant upper thermospheric contribution to the O($^1$S) 557.7 nm dayglow emission: First ground based evidence, *J. Atmos. Sol. Terr. Phys.*, *65*, 121–128.

Tapping, K. (1987), Recent solar radio astronomy at centimeter wavelengths: The temporal variability of the 10.7-cm flux, *J. Geophys. Res.*, *92*, 829–838.

Thuillier, G., R. H. Wiens, G. G. Shepherd, and R. G. Roble (2002), Photochemistry and dynamics in thermospheric intertropical arcs measured by the WIND Imaging Interferometer on board UARS: A comparison with TIE-GCM simulations, *J. Atmos. Sol. Terr. Phys.*, *64*, 405–415.

Upadhayaya, A. K., and V. Singh (2002), Effects of temperature dependence of reaction $N_2(A^3\Sigma_u^+)$ on greenline dayglow, *Ann. Geophys.*, *20*, 2039–2045.

Ward, W. E. (1999), A simple model of diurnal variations in the mesospheric oxygen nightglow, *Geophys. Res. Lett.*, *26*, 3565–3568.

Ward, W. E., B. Solheim, and G. G. Shepherd (1997), Two day wave induced variations in the oxygen green line volume emission rate: WINDII variations, *Geophys. Res. Lett.*, *24*, 1127–1130.

Witasse, O., J. Lilensten, C. Lathuillere, and P. L. Blelly (1999), Modeling the OI 630.0 and 557.7 nm thermospheric dayglow during EISCAT-WINDII coordinated measurements, *J. Geophys. Res.*, *104*, 24,639–24,655.

Woods, T. N., W. K. Tobiska, G. J. Rottman, and J. R. Worden (2000), Improved solar Lyman α irradiance modeling from 1947 through 1999 based on UARS observations, *J. Geophys. Res.*, *105*, 27,195–27,215.

Woods, T. N., F. G. Eparvier, S. C. Solomon, D. L. Woodraska, and S. M. Bailey (2003), Early results from the TIMED Solar EUV Experiment, paper presented at the 4th TIGER Symposium,Fraunhofer-Inst. für Phys. Messtechnik. (Available at http://www.ipm.fhg.de/english/meetings/workshops/tiger/documents/p_woods_results_TIMED_experiment.pdf)

Zhang, S.-P., R. G. Roble, and G. G. Shepherd (2001), Tidal Influence on the oxygen and hydroxyl nightglows: WINDII observations and TIME-GCM simulations, *J. Geophys. Res.*, *106*, 21,381–21,394.

R. Maharaj-Sharma, University of the West Indies, St. Augustine, Trinidad and Tobago.

G. G. Shepherd, Centre for Research in Earth and Space Science, York University, Toronto, Canada M3J 1P3. (gordon@yorku.ca)